Proceedings of "Applications of Physics in Mechanical and Material Engineering" (APMME 2024)

The Dynamic Stability of Quasi-Periodic and Aperiodic Multi-Segment Columns

S. Garus*, W. Sochacki, D. Leśniak and J. Garus

Department of Mechanics and Fundamentals of Machinery Design, Faculty of Mechanical Engineering, Czestochowa University of Technology, Dąbrowskiego 73, 42-201 Częstochowa, Poland

Doi: 10.12693/APhysPolA.147.176 *e-mail: sebastian.garus@pcz.pl

In this work, Bernoulli–Euler columns, freely supported and loaded by a longitudinal force variable over time, are considered. The problem of dynamic stability is solved using the mode summation method. The applied research procedure allows the dynamics of the tested system to be described using the Mathieu equation. The influence of stiffness distribution in the Bernoulli–Euler beam on the value of coefficient b in the Mathieu equation is investigated. Structures are created using deterministic rules such as substitution rule, generation rule, recursion or inflation rule. The quasi-periodic structures that are taken into account are: the Fibonacci chain, the silver Fibonacci chain, the bronze Fibonacci chain, the octagonal chain, and the dodecagonal chain. The aperiodic structures that are taken into account are: the Severin chain, the Thue–Morse chain, the copper Fibonacci chain, the nickel Fibonacci chain, and the circular chain. The results obtained on the basis of numerical tests for structures with variable stiffness of the considered columns will be analyzed in order to compare and distinguish the factors that have the greatest impact on the change of natural frequencies and on the dynamic stability of the columns under consideration.

topics: dynamic stability, Strutt card, Mathieu equation, multi-segment columns

1. Introduction

Many machine elements in mechanical engineering can be modeled using Bernoulli–Euler beams, but as slender elements subjected to a time-varying axial force, they may, under certain circumstances, be susceptible to the occurrence of parametric resonance phenomena, which may ultimately lead to the destruction of the system. By using appropriate clamps, it is possible to increase the stiffness of the beam locally and thus create a system with variable stiffness.

Parametric resonance occurs in many types of physical phenomena [1–7]. Its analysis is possible after transforming it into the form of the Mathieu equation of motion [8–13], which can take stable and unstable solutions [14].

Investigating the influence of aperiodic and quasi-periodic structures and learning about the influence of these distributions on parameters of great importance in the safety of structures and devices may open the possibility of using structures with a non-periodic order in much more complex solutions used in industry. Mechanical engineering, as a field dealing with the design, manufacture, and operation of machines and structures, is constantly looking for new solutions that are safer and more economical in production. The use of structures with non-periodic distribution may allow for the shift of dangerous resonance frequencies. In the case of promising results from the study of column systems, it will also be important to carry out a future analysis of the influence of structures with more than one dimension.

So far, the aperiodic and quasi-periodic distribution of segments in columns has not been used in constructions and machines, and it is assumed that the influence of this distribution on the properties of the column is significant, especially in situations where the column is loaded with a periodic force, where despite a low value of the force, the system may be damaged due to the effect of the parametric resonance phenomenon.

2. Methodology

The Bernoulli–Euler beam loaded with an axial compressive force with variable stiffness for the exemplary $XYXYX$ distribution is shown in Fig. 1. The constant component of the load is P_0, the variable component of the load is S, time is marked by t, the frequency of the exciting force is ν, the

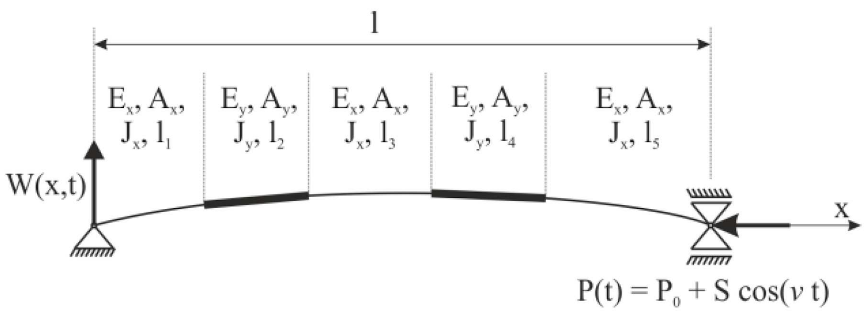

Fig. 1. Example of a variable stiffness beam (XYXYX) loaded with an axial compressive force varying in time.

Young modulus is E, section moment of inertia is J, cross-sectional area is A, and the material density is ρ. The subscripts correspond to the given layer X or Y.

Using Hamilton's variational principle

$$\delta \int_{t_1}^{t_2} \mathrm{d}t\ (T-V)=0, \tag{1}$$

for which the kinetic energy was defined by

$$T=\sum_{i=1}^{N}\frac{1}{2}\int_0^l \mathrm{d}x\ \rho_i A_i\left(\frac{\partial W_i(x,t)}{\partial t}\right)^2, \tag{2}$$

while the potential energy as

$$V=\sum_{i=1}^{N}\frac{1}{2}\int_0^l \mathrm{d}x\ E_iJ_i\left(\frac{\partial^2 W_i(x,t)}{\partial x^2}\right)^2 -\sum_{i=1}^{N}\frac{1}{2}P(t)\int_0^l \mathrm{d}x\ \left(\frac{\partial W_i(x,t)}{\partial x}\right)^2, \tag{3}$$

the equation of motion of the column was obtained in the form

$$E_iJ_i\frac{\partial^4 W_i(x,t)}{\partial x^4}+\rho_iA_i\frac{\partial^2 W_i(x,t)}{\partial t^2} +P(t)\frac{\partial^2 W_i(x,t)}{\partial x^2}=0. \tag{4}$$

The solution of (4) was assumed as a sum of eigenfunctions in the form

$$W_i(x,t)=\sum_{n=1}^{\infty}W_{i,n}(x)\,T_{i,n}(t), \tag{5}$$

where adopting $T_{i,1}(t)=\cos(\omega_{i,1}t)$ and assuming that the first term of the sum is of the greatest importance after separating the variables, allowed to obtain

$$\frac{\partial^4 W_i(x)}{\partial x^4}+\frac{P}{E_iJ_i}\frac{\partial^2 W_i(x)}{\partial x^2}-\frac{\rho_iA_i\omega_{i,1}^2}{E_iJ_i}W_i(x)=0, \tag{6}$$

and the solution to this equation was the function

$$W_i(x)= C_{i,1}\cosh\left(x\sqrt{-\frac{P}{2E_iJ_i}+\sqrt{\left(\frac{P}{2E_iJ_i}\right)^2+\frac{\rho_iA_i\omega_{i,1}^2}{E_iJ_i}}}\right)+C_{i,2}\sinh\left(x\sqrt{-\frac{P}{2E_iJ_i}+\sqrt{\left(\frac{P}{2E_iJ_i}\right)^2+\frac{\rho_iA_i\omega_{i,1}^2}{E_iJ_i}}}\right) +C_{i,3}\cos\left(x\sqrt{\frac{P}{2E_iJ_i}+\sqrt{\left(\frac{P}{2E_iJ_i}\right)^2+\frac{\rho_iA_i\omega_{i,1}^2}{E_iJ_i}}}\right)+C_{i,4}\sin\left(x\sqrt{\frac{P}{2E_iJ_i}+\sqrt{\left(\frac{P}{2E_iJ_i}\right)^2+\frac{\rho_iA_i\omega_{i,1}^2}{E_iJ_i}}}\right). \tag{7}$$

The geometric and natural boundary conditions were

$$W_1(0)=W_N(l)=0, \tag{8}$$

$$E_iJ_i\frac{\mathrm{d}^2W_1(0)}{\mathrm{d}x^2}=0, \tag{9}$$

$$E_iJ_i\frac{\mathrm{d}^2W_N(l)}{\mathrm{d}x^2}=0, \tag{10}$$

whereas the continuity conditions are defined as

$$W_i(x)=W_{i+1}(x), \tag{11}$$

$$\frac{\mathrm{d}W_i(x)}{\mathrm{d}x}=\frac{\mathrm{d}W_{i+1}(x)}{\mathrm{d}x}, \tag{12}$$

$$E_iJ_i\frac{\mathrm{d}^2W_i(x)}{\mathrm{d}x^2}=E_{i+1}J_{i+1}\frac{\mathrm{d}^2W_{i+1}(x)}{\mathrm{d}x^2}, \tag{13}$$

and

$$E_i J_i \frac{\mathrm{d}^3 W_i(x)}{\mathrm{d}x^3} = E_{i+1} J_{i+1} \frac{\mathrm{d}^3 W_{i+1}(x)}{\mathrm{d}x^3}. \tag{14}$$

By substituting (7) and its appropriate derivatives into the conditions of (8)–(14), a system of equations in the matrix form was obtained for the unknown constants $C_{i,j}$ as

$$[M](\omega)\, C = 0, \tag{15}$$

where $[M](\omega) = [a_{pq}]$, $[p,q] = (1,\ldots,4)$, and $C = [C_{ij}]^{\mathrm{T}}$, $i = 1,\ldots,N$, $j = 1,\ldots,4$.

A non-trivial solution was obtained by equating the value of the determinant of the M matrix to zero, which enabled the determination of the natural frequencies ω_i for a given load P and the determination of the critical force P_k of the analyzed system.

In this work, the orthogonality of eigenfunctions was assumed, and the condition that had to be met was determined as

$$\sum_{i=1}^{N} \left[\rho_i^* \int_0^l \mathrm{d}x\; W_{i,n}(x)\, W_{i,m}(x) \right] = \begin{cases} 0, & m \neq n; \\ \gamma_m^2 = \sum_{i=1}^{N} \left[\int_0^l \mathrm{d}x\; W_i^2(x) \right] & m = n. \end{cases} \tag{16}$$

Then, the equation of motion (4) was transformed into the Mathieu equation, and the following was obtained

$$\frac{\partial^2 T(\tau)}{\partial \tau^2} + \left(\frac{-\omega_i^2}{\nu^2} + \frac{\sum\limits_{i=1}^{N} \int\limits_0^l \frac{\partial^2 W_i(x)}{\partial x^2} W_i(x)\,\mathrm{d}x}{\sum\limits_{i=1}^{N} \rho_i A_i \int\limits_0^l W_i^2(x)\,\mathrm{d}x} \frac{S}{\nu^2} \cos\tau \right) T(\tau) = 0, \tag{17}$$

where $\tau = \nu t$ and

$$a = \frac{-\omega_i^2}{\nu^2}, \tag{18}$$

$$b = b_1 \frac{S}{\nu^2} = \frac{\sum\limits_{i=1}^{N} \int\limits_0^l \mathrm{d}x\; \frac{\partial^2 W_i(x)}{\partial x^2} W_i(x)}{\sum\limits_{i=1}^{N} \rho_i A_i \int\limits_0^l \mathrm{d}x\; W_i^2(x)} \frac{S}{\nu^2}. \tag{19}$$

The obtained equation of motion in the form of the Mathieu equation (17) can be written as

$$\frac{\partial^2 y(t)}{\partial t^2} + (a + b\cos(t))\, y(t) = 0. \tag{20}$$

The solution of (20), depending on parameters a and b, can be stable and unstable. The distribution of stable and unstable areas of solutions to the Mathieu equation, depending on parameters a and b, is shown in the Strutt chart in Fig. 2. The stable areas are marked in white, and non-stable areas in grey.

In Fig. 2., two points are marked, namely blue in the area of unstable solutions and red in the area of stable solutions. By inserting the appropriate values of coefficients a and b for the selected points, solutions to (20) in time were obtained by Mathieu's equation, as shown in Fig. 3. Appropriate solutions for selected points are marked with corresponding colors. As can be seen, the solution for the blue point, located in the unstable region, tends exponentially to infinity, which means that parametric resonance occurs for the analyzed parameters, and the tested system may be destroyed. On the other hand, the solution for the red point, for parameters a and b in the area of stable solutions, is periodic, and there is no parametric resonance.

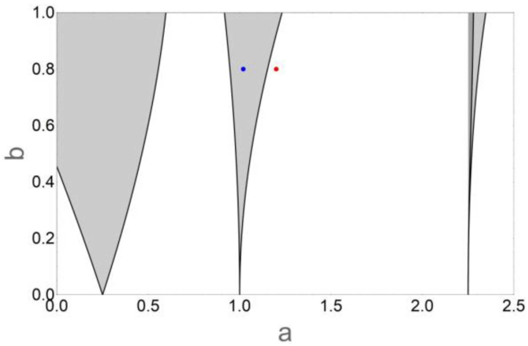

Fig. 2. Strutt chart describing the stable (white) and unstable (grey) areas of solutions to the Mathieu equation depending on the parameters a and b.

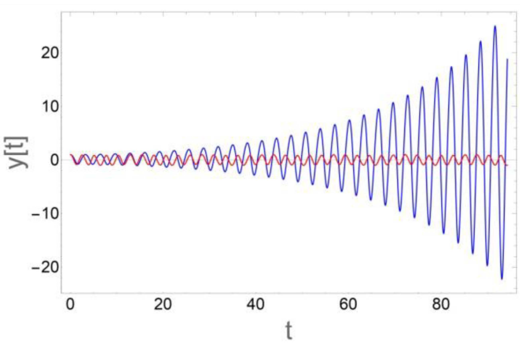

Fig. 3. Solutions of Mathieu's equations with parameters a and b selected from the range of stable (red) and unstable (blue) solutions.

TABLE I

Analyzed structures.

Type	Analyzed structures	Symbol	n	Stiffness distributions
periodic	binary chain	C^{B}	5	XYXYXYXYXY
quasi-periodic	Fibonacci chain	C^{F}	5	YXYXYYXY
	silver Fibonacci chain	C^{SF}	4	XXYXXYYYXXY
	bronze Fibonacci chain	C^{BF}	3	YYYXXXY
	octagonal chain	C^{O}	3	XYXYXXYXYXXY
	dodecagonal chain	C^{D}	4	YYYXYYYXYYX
aperiodic	Severin chain	C^{S}	3	XYXYYYXY
	Thue–Morse chain	C^{TM}	3	XYYXYXXY
	copper Fibonacci chain	C^{CF}	3	YXXYYYXXYXX
	nickel Fibonacci chain	C^{NF}	2	YXXXYYY
	circular chain	C^{C}	2	YYXYXXYXYYXYX

3. Analyzed structures

The work will analyze different types of structures. Structures are created using deterministic rules such as substitution rule, generation rule, recursion, or inflation rule. Pattern a_n specifies the sequence that corresponds to the n-th step of the deterministic rule.

A binary structure is a kind of periodic structure [15]. For the initial value $a_0 = XY$, where the parameters X and Y symbolize a given type of Bernoulli–Euler segment and the superscript denotes the number of times the sequence is repeated, the successive steps are described by the formula

$$a_n = (a_0)^n. \tag{21}$$

The quasi-periodic structures include the Fibonacci chain [16–19], the silver Fibonacci chain [20], the bronze Fibonacci chain [20], the octagonal chain [21, 22], and the dodecagonal chain [21].

The aperiodic structures include the Severin chain [23, 24], the Thue–Morse chain [25–29], the copper Fibonacci chain [20], the nickel Fibonacci chain [20], and the circular chain [30–32].

The deterministic rules for the formation of subsequent structures are presented below.

Sample initial conditions for Fibonacci chains are

$$\begin{cases} a_0 = X \\ a_1 = Y \end{cases}. \tag{22}$$

The recursive method of obtaining the Fibonacci sequence is given by

$$a_{n+1} = a_n a_{n-1}. \tag{23}$$

The recursive method of obtaining the silver Fibonacci sequence is

$$a_{n+1} = a_n a_n a_{n-1}. \tag{24}$$

The recursive method of obtaining the bronze Fibonacci sequence is

$$a_{n+1} = a_n a_n a_n a_{n-1}. \tag{25}$$

In the dodecagonal chain, we also assume the initial conditions presented in (22), while the steps of creating the structure depend on the parity of the step number, i.e.,

$$\begin{cases} a_n = a_{n-1} a_{n-2} a_{n-2}, & n = 2m; \\ a_n = a_{n-2} a_{n-2} a_{n-2} a_{n-3}, & n = 2m+1. \end{cases} \tag{26}$$

The rule of octagonal chain generation can be represented as

$$a_{n+1} = a_n a_n a_{n-1}, \tag{27}$$

for initial conditions

$$\begin{cases} a_0 = X, \\ a_1 = XY. \end{cases} \tag{28}$$

In order to find the distribution in the Severin structure, the following substitution rule should be used

$$\begin{cases} Y \to XY, \\ X \to YY, \end{cases} \tag{29}$$

for the initial value

$$a_0 = Y. \tag{30}$$

The Thue–Morse chain for the initial conditions in (28) is also formed based on the substitution rule

$$\begin{cases} Y \to YX, \\ X \to XY. \end{cases} \tag{31}$$

The copper Fibonacci chain can be determined according to the following substitution rule

$$\begin{cases} X \to Y, \\ Y \to YXX, \end{cases} \tag{32}$$

while the Fibonacci nickel chain was defined by

$$\begin{cases} X \to Y, \\ Y \to YXXX. \end{cases} \tag{33}$$

In both cases, the starting value for generating the chains is

$$a_0 = X. \tag{34}$$

TABLE II

Eigenfrequencies and masses of beams with a constant cross-section.

	A_X	$2A_X$	$3A_X$
A [m^2]	0.09	0.18	0.27
M [kg]	2122.2	4244.4	6366.6
ω_1 $\left[\frac{\text{rad}}{\text{s}}\right]$	489.31	693.668	849.946
ω_2 $\left[\frac{\text{rad}}{\text{s}}\right]$	1961.99	2776.35	3400.7
ω_3 $\left[\frac{\text{rad}}{\text{s}}\right]$	4416.45	6247.48	7651.95
ω_4 $\left[\frac{\text{rad}}{\text{s}}\right]$	7852.7	11107.1	13603.7

A circular chain can be obtained using a three-element substitution rule

$$\begin{cases} x \to zxz, \\ y \to xzzxz, \\ z \to xyzxz. \end{cases} \tag{35}$$

The distribution of the beams in the column is obtained on the basis of the following identification rule

$$\begin{cases} x, y \to Y, \\ z \to X, \end{cases} \tag{36}$$

for the initial value

$$a_0 = x. \tag{37}$$

Based on the above rules, subsequent types of beam distribution in the column are obtained.

Structures with the maximum n-th step of the deterministic rule were selected for the analysis, so that the structure meets the assumptions of using Bernoulli–Euler beams. The beam stiffness distributions selected for the analysis are summarized in Table I.

4. Solving the boundary problem

The zero points of the determinants make it possible to determine the eigenfrequencies of the analyzed beams. They have been collected in Tables II–IV and are a solution to the boundary problem.

The work analyzed Bernoulli–Euler beams with the stiffness distribution presented in Table I. The beam length of $3m$ was assumed for the calculations. The length of the beam subsection with n elements was L/n. The entire column was made of a homogeneous material — steel (Young's modulus $E = 2.1 \times 10^{11}$ Pa, density $\rho = 7.86 \times 10^3$ kg/m^3). The static part of the load was $P = 10^6$ N. The cross-section of segment X was a square with a side of $0.3m$ and area A_X. The cross-section of segment Y was a square whose cross-sectional area $A_Y = 2A_X$ (Table III) and $A_Y = 3A_X$ (Table IV).

TABLE III

Masses and eigenfrequencies for the analyzed structures in the case of a ratio of cross-sections of $A_Y = 2A_X$.

Structure	Mass [kg]	ω_1 $\left[\frac{\text{rad}}{\text{s}}\right]$	ω_2 $\left[\frac{\text{rad}}{\text{s}}\right]$	ω_3 $\left[\frac{\text{rad}}{\text{s}}\right]$	ω_4 $\left[\frac{\text{rad}}{\text{s}}\right]$
C^{O}	3006.45	495.934	2006.63	4536.59	8144.36
C^{BF}	3334.89	504.527	2323.38	5155.31	9217.69
C^{NF}	3334.89	504.527	2323.38	5155.31	9217.69
C^{C}	3264.92	506.472	2091.86	4656.70	8474.36
C^{B}	3183.30	506.816	2041.17	4636.70	8333.05
C^{TM}	3183.30	510.553	2145.29	4884.37	8404.50
C^{SF}	3086.84	519.744	2035.48	4754.92	8895.47
C^{CF}	3086.84	519.744	2035.48	4754.92	8895.47
C^{F}	3448.58	526.402	2099.11	4581.79	9427.40
C^{D}	3665.62	558.788	2198.29	5864.27	9593.03
C^{S}	3448.58	560.652	2096.59	5236.24	9149.87

TABLE IV

Masses and eigenfrequencies for the analyzed structures in the case of a ratio of cross-sections of $A_Y = 3A_X$.

Structure	Mass [kg]	ω_1 $\left[\frac{\text{rad}}{\text{s}}\right]$	ω_2 $\left[\frac{\text{rad}}{\text{s}}\right]$	ω_3 $\left[\frac{\text{rad}}{\text{s}}\right]$	ω_4 $\left[\frac{\text{rad}}{\text{s}}\right]$
C^{O}	3890.7	456.905	1861.16	4274.27	7797.62
C^{B}	4244.4	466.429	1888.58	4334.26	7903.39
C^{C}	4407.65	467.138	1958.18	4347.93	8187.17
C^{TM}	4244.4	473.571	2092.12	4809.06	8031.88
C^{BF}	4547.57	476.649	2408.47	5756.94	9574.73
C^{NF}	4547.57	476.649	2408.47	5756.94	9574.73
C^{SF}	4051.47	484.051	1922.85	4624.73	9466.69
C^{CF}	4051.47	484.051	1922.85	4624.73	9466.69
C^{F}	4774.95	490.732	1977.79	4326.51	10031.8
C^{D}	5209.04	536.033	2097.72	6480.60	10277.1
C^{S}	4774.95	540.113	1974.61	5442.22	9668.61

First, the eigenfrequencies and masses of beams with a constant cross-section were determined (Table II). Along with the increase in the cross-section A [m^2], the beam masses m [kg] increased proportionally. Subsequent natural frequencies ω_i $\left[\frac{\text{rad}}{\text{s}}\right]$ also increased.

Tables III and IV show the determined beam masses and eigenfrequencies for the ratio of $A_Y = 2A_X$ and $A_Y = 3A_X$ cross-sections, respectively. These tables are sorted according to the increasing value of the first eigenfrequency ω_1. The lowest values of all eigenfrequencies were characterized by the quasi-periodic octagonal chain C^{O}, which also had the lowest mass. The structures

TABLE V

Determined values of critical force and coefficient b (for $a = 1$) for the analyzed structures.

Type	Analyzed structures	Symbol	$P_C \times 10^6$ [N]		$b \times 10^{-8}$	
			$A_Y = 2A_X$	$A_Y = 3A_X$	$A_Y = 2A_X$	$A_Y = 3A_X$
periodic	binary chain	C^{B}	247	278	8.567	10.508
quasi-periodic	Fibonacci chain	C^{F}	280	327	5.757	6.806
	silver Fibonacci chain	C^{SF}	260	295	9.882	12.029
	bronze Fibonacci chain	C^{BF}	207	217	4.511	4.723
	octagonal chain	C^{O}	221	240	10.885	13.093
	dodecagonal chain	C^{D}	344	440	6.951	7.969
aperiodic	Severin chain	C^{S}	337	422	5.984	7.079
	Thue–Morse chain	C^{TM}	242	268	6.746	8.153
	copper Fibonacci chain	C^{CF}	260	295	9.889	12.045
	nickel Fibonacci chain	C^{NF}	207	217	4.509	4.721
	circular chain	C^{C}	242	270	10.452	12.576

of C^{BF} and C^{NF} stiffness distribution, as well as C^{SF} and C^{CF}, were respectively symmetric to each other, which resulted in exactly the same values of masses and eigenfrequencies.

In the C^{F} and C^{S} structures, despite the identical mass of the beams, there were clear differences in the values of eigenfrequencies; only the values of the second eigenfrequency were similar in both analyzed cases. Identical masses were also found in C^{B} and C^{TM} structures, but in this case, none of the eigenfrequencies were close to each other. Increasing the cross-sections, and thus the mass, for the structures from Table IV in relation to the data from Table III resulted in a decrease in the value of the first natural frequency, which is contrary to the relationship resulting from the increase in the cross-section of the beams from Table II. Despite the same or higher masses of selected structures from Table IV, the values of the first natural frequencies were significantly lower in relation to the beam with a constant $2A_X$ cross-section from Table II.

5. Analysis of the critical force and dynamic stability of beams

In Table V, the determined values of the critical force P_C for the analyzed periodic, quasi-periodic, and aperiodic distributions of the Bernoulli–Euler beam stiffness and the coefficient b from the equation of motion in the form of the Mathieu equation (for coefficient a equal to 1) are presented.

For stiffness distributions where $A_Y = 2A_X$, the minimum values of the critical force were 207×10^6 N for the bronze Fibonacci chain and nickel Fibonacci chain (these are the same structures, but differently oriented in relation to the time-varying force). Similarly, for $A_Y = 3A_X$, the same structures were characterized by the lowest values of the critical force. However, the highest value of the critical force was characterized by the dodecagonal chain structure, which for $A_Y = 3A_X$ was 440×10^6 N and was more than twice as high as the minimum value, while for $A_Y = 2A_X$, it was 344×10^6 N. For all the analyzed structures, the critical force had a higher value when $A_Y = 3A_X$.

The higher the value of the coefficient b of the Mathieu equation, the more unstable the system is for larger frequency ranges of the excitation force. As part of the research, it was shown that the bronze Fibonacci chain and nickel Fibonacci chain structures showing the lowest critical force values were also characterized by greater dynamic stability. However, the relationship between the critical force and dynamic stability has not been shown. The most unstable structure of the stiffness distribution was the octagonal chain, whose critical strength did not differ much from the most stable structures. The heaviest of the analyzed Bernoulie–Euler beams with the dodecagonal chain stiffness distribution structure, despite the highest values of the critical force, did not show extreme values of the coefficient b of the Mathieu equation.

6. Conclusions

In the research, the properties of Bernoulie–Euler beams with variable stiffness, which were subjected to an axial force varying in time, were analyzed. Eleven stiffness distributions were analyzed, divided into three groups: periodic (binary chain), quasi-periodic (Fibonacci chain, silver Fibonacci chain, bronze Fibonacci chain, octagonal chain, dodecagonal chain), and aperiodic (Severin chain, Thue–Morse chain, copper Fibonacci chain, nickel Fibonacci chain, circular chain).

The carried out research allowed us to determine the stiffness distributions for the analyzed structures, and the adopted solution for the obtained equation of motion inserted into the natural and geometric boundary conditions and continuity conditions allowed us to determine the eigenfrequencies. By inserting one for the first integration constant of the first shape function, the remaining integration constants were obtained, and the shape functions for the considered beams were determined. By determining the zeros of the determinant of the matrix M for the successive values of the force, P–ω diagrams were developed, and on their basis, the values of the critical force of the analyzed structures were determined. Using the integrals of the shape function, parameters a and b of the Mathieu equation were determined, on the basis of which the dynamic stability of the considered beams was analyzed.

The conducted tests showed that increasing the stiffness of a structure element increased its critical force, but there was no relationship between the critical force and the stability of the structure. The stiffness distribution significantly affected the shape functions. The structures of the bronze Fibonacci chain and nickel Fibonacci chain, which had the same distribution for the considered generation number, turned out to be the most stable. The next most stable structures were the Fibonacci chain within quasi-periodic structures and the Severin chain within aperiodic structures. The least static was the quasi-periodic octagonal chain structure. On the other hand, the periodic structure was not characterized by high dynamic stability within the analyzed structures.

The tests carried out showed a significant influence of the stiffness distribution on the dynamic stability and the lack of a clear correlation between the dynamic stability and the mass or critical force in the analyzed beams. The lack of simple correlations and the high possibility of stiffness distributions (large space of possible states) suggest the need to use heuristic algorithms (e.g., genetic algorithm) to determine the distribution with the most optimal parameters (minimization of the coefficient b of the Mathieu equation) in order to increase the dynamic stability of the considered beams.

The obtained results indicate that local increases in the stiffness of the beam (e.g., in the form of clamps) significantly affect the nature of natural vibrations. This phenomenon can greatly affect the occurrence of parametric resonance, and the appropriate use of structural elements that increase stiffness can lead to increased safety of the structure.

References

[1] Y.K. Lin, G.Q. Cai, *Probabilistic Structural Dynamics*, McGraw-Hill, New York 1995.

[2] L.D. Landau, E.M. Lifshitz, *Mechanics*, Elsevier, Oxford 2007.

[3] J.J.H. Brouwers, *Phys. D Nonlinear Phenom.* **240**, 990 (2011).

[4] A.H. Nayfeh, D.T. Mook, *Nonlinear Oscillations*, Wiley, New York 1979.

[5] D. Yurchenko, A. Naess, P. Alevras, *Probabilistic Eng. Mech.* **31**, 12 (2013).

[6] Z.H. Feng, X.J. Lan, X.D. Zhu, *Int. J. Non-Linear Mech.* **42**, 1170 (2007).

[7] G. Song, V. Sethi, H.-N. Li, *Eng. Struct.* **28**, 1513 (2006).

[8] C.-Y. Lin, L.-W. Chen, *J. Sound Vib.* **267**, 209 (2003).

[9] W. Sochacki, *Thin-Walled Struct.* **45**, 927 (2007).

[10] Y. Li, S. Fan, Z. Guo, J. Li, L. Cao, H. Zhuang, *Commun. Nonlinear Sci. Numer. Simul.* **18**, 401 (2013).

[11] Y. Zhou, Y. Zhang, G. Yao, *Compos. Struct.* **267**, 113858 (2021).

[12] W. Sochacki, *J. Sound Vib.* **314** 180 (2008).

[13] Y.-S. Shih, Z.-F. Yeh, *Int. J. Solids Struct.* **42**, 2145 (2005).

[14] G.N. Jazar, *Int. J. Non-Linear Mech.* **39**, 1319 (2004).

[15] S. Garus, W. Sochacki, *J. Appl. Math. Comput. Mech.*, **17**, 19 (2018).

[16] D. Levine, P.J. Steinhardt, *Phys. Rev. Lett.* **53**, 2477 (1984).

[17] J.Q. You, Q.B. Yang, *J. Phys. Condens. Matter* **2**, 2093 (1990).

[18] J.Q. You, J.R. Yan, T. Xie, X. Zeng, J.X. Zhong, *J. Phys. Condens. Matter* **3**, 7255 (1991).

[19] Y. Errouas, Y. Ben-Ali, A. Ouariach, Z. Tahri, D. Bria, *Mater. Today Proc.* **27**, 3058 (2020).

[20] G. Gumbs, M.K. Ali, *Phys. Rev. Lett.* **60**, 1081 (1988).

[21] J.E.S. Socolar, *Phys. Rev. B* **39**, 10519 (1989).

[22] S. Garus, M. Bold, W. Sochacki, *Acta Phys. Pol. A* **135**, 139 (2019).

[23] M. Severin, M. Dulea, R. Riklund, *J. Phys. Condens. Matter* **1**, 8851 (1989).

[24] S. Garus, W. Sochacki, *J. Appl. Math. Comput. Mech.* **16**, 17 (2017).

[25] C.S. Ryu, G.Y. Oh, M.H. Lee, *Phys. Rev. B* **48**, 132 (1993).

[26] J.X. Zhong, J.R. Yan, J.Q. You, *J. Phys. Condens. Matter* **3**, 6293 (1991).

[27] M. Kolář, M.K. Ali, F. Nori, *Phys. Rev. B* **43**, 1034 (1991).

[28] H. Ni, J. Wang, A. Wu, *Optik* **242**, 167163 (2021).

[29] Y. Trabelsi, N. Ben Ali, F. Segovia-Chaves, H. V. Posada, *Results Phys.* **19**, 103600 (2020).

[30] S. Aubry, C. Godrèche, J.M. Luck, *Europhys. Lett.* **4**, 639 (1987).

[31] J. M. Luck, *Phys. Rev. B* **39**, 5834 (1989).

[32] C. Godreche, J. M. Luck, *J. Phys. Math. Gen.* **23**, 3769 (1990).